Published in final edited form as:
Biomaterials. 2008 March ; 29(8): 1065–1074.

EFFECTS OF DECELLULARIZATION ON THE MECHANICAL AND STRUCTURAL PROPERTIES OF THE PORCINE AORTIC VALVE LEAFLET

Jun Liao[1], **Erinn M. Joyce**[1], and **Michael S. Sacks**[2]
From the Engineered Tissue Mechanics and Mechanobiology Laboratory, Department of Bioengineering and McGowan Institute for Regenerative Medicine, University of Pittsburgh, Pittsburgh PA 15219

Abstract

The potential for decellularized aortic heart valves (AVs) as heart valve replacements is based on the assumption that the major cellular immunogenic components have been removed, and that the remaining extracellular matrix (ECM) should retain the necessary mechanical properties and functional design. However, decellularization processes likely alter the ECM mechanical and structural properties, potentially affecting long term durability. In the present study we explored the effects of an anionic detergent (SDS), enzymatic agent (Trypsin), and a non-ionic detergent (Triton X-100) on the mechanical and structural properties of AV leaflets (AVLs) to provide greater insight into the initial functional state of the decellularized AVL. The overall extensibility represented by the areal strain under 60 N/m increased from 68.85% for the native AV to 139.95%, 137.51%, and 177.69% for SDS, Trypsin, and Triton X-100, respectively, after decellularization. In flexure, decellularized AVLs demonstrated a profound loss of stiffness overall, and also produced a nonlinear moment-curvature relation compared to the linear response of the native AVL. Effective flexural moduli decreased from 156.0±24.6 kPa for the native AV to 23.5±5.8 kPa, 15.6±4.8 kPa, and 19.4 ±8.9 kPa for SDS, Trypsin, and Triton X-100 treated leaflets, respectively. While the overall leaflet fiber architecture remained relatively unchanged, decellularization resulted in substantial microscopic disruption. In conclusion, changes in mechanical and structural properties of decellularized leaflets were likely associated with disruption of the ECM, which may impact the durability of the leaflets.

INTRODUCTION

The aortic valve (AV) consists of three leaflets (often referred to in the literature as cusps due to their shape) that permit unidirectional blood to flow from the left ventricle to the aorta. Structurally, the AV leaflet (AVL) consists of the fibrosa, spongiosa, and ventricularis layers. The fibrosa layer, which faces the aorta, is primarily composed of Type I collagen fibers with a strong preferred circumferential orientation. The ventricularis, which faces the left ventricle, is composed of elastin and collagen. The spongiosa, located between the fibrosa and the ventricularis, is mainly composed of glycosaminoglycans and water [1]. The AV is capable of withstanding 30–40 million cycles per year, resulting in a total of ~3 billion cycles in a single

[2]For correspondence: Michael S. Sacks, Ph.D., W.K. Whiteford Professor, 100 Technology drive, Room 234, University of Pittsburgh, Pittsburgh, PA 15219, Tel: 412-235-5146, Fax: 412-235-5160, email: msacks@pitt.edu.
[1]Both co-authors contributed equally to this work.

lifetime [1]. The astonishing performance of the AV can be interrupted by AV disease, and needs to be repaired or replaced to avoid cardiopulmonary failure or death [2]. At least 60,000 substitute valves are implanted in the United States and 170,000 world wide each year [3].

Currently, mechanical and bioprosthetic heart valves (BHV) are the major valve substitute types. Mechanical valves have a functional life span of at least 25 years but are associated with a substantial risk of thromboembolism and life-long anticoagulation treatment [4]. BHVs have better hemodynamic characteristics and avoid long-term anticoagulation therapies but suffer from structural dysfunction due to progressive tissue deterioration [5]. Also, all clinically used tissue valve substitutes are nonviable, and thus, they have no potential to grow, to repair, or to remodel. Therefore, their capability is limited, especially in growing children [6,7].

Cellular remnants within treated BHV tissues have been found to form the nidus for calcification and related immunological responses [8–14]. Thus, decellularization of the AV potentially attenuates calcification and immunological responses [10,11,13,14]. Moreover, it was found that natural ligands and ECM constituents of decellularized valve tissues benefit cell attachment, endothelialization, and tissue reconstitution [15]. Based on these results, decellularized AVs, wherein the interstitial cells have been extracted through tissue decellularization, have been explored as used for valve replacement [15–22]. Decellularized native valve tissues, unlike synthetic scaffold approaches [6,23,24], have the potential to be readily used for AV replacements since they are assumed to have the necessary mechanical strength and the inherent functional design [15–22].

Various detergents or enzymatic agents have been used to remove cells and cellular debris in valved conduits. Commonly used decellularization methods are a non-ionic detergent, Triton X-100, (tert-octylphenylpolyoxyethylen) [16,21,25], an anionic detergent, SDS (sodium dodecyl sulfate) [20], and an enzymatic agent, Trypsin [15,18,22,26,27]. To understand the mechanics of decellularized valve leaflets, Korossis et al [20] measured the leaflet strips cut along the circumferential or the radial direction and found that after treatment with SDS (hypotonic buffer), extensibility and failure strain of circumferential strips significantly increased, while in the radial strips, there was some increase but not significantly [20]. Although the tensile modulus decreased, ultimate tensile strengths of both circumferential and radial specimens did not decrease after SDS treatment [20]. Similarly, Spina et al. [28] reported that after decellularization with either Triton X-100 (with cholate) or N-cetylpyridinium extraction, only circumferential specimens exhibited ~20% higher extensibility and had a ~10% lower stiffness. Other parameters such as extensibility and stiffness in radial direction and failure strain, failure strength, and relaxation slope of both circumferential and radial specimen were not significantly different [28].

The above studies suggest that decellularization procedures introduce some changes, but may not compromise tissue mechanical strength and performance [20,28]. However, even if the ultimate tensile strength was not compromised [20,28], it does not mean that acellular valvular tissues will perform the same way as the native tissue in the physiological range. In general, it is unclear as to how valvular function is affected by the decellularization process. Further, if recellularization and tissue maintenance do not occur in vivo, it is crucial to determine how long the decellularized AV will function.

To address these issues, an understanding of the mechanical and microstructural defects induced by decellularization of the AVL, and establishing functional limits of the decellularized AV. Thus, there is a need for in-depth studies of the mechanical and structural properties of the decellularized leaflets in the physiological functional range. In the present study, we conducted biaxial and flexural mechanical testing, SALS, and histological analyses to investigate the defects caused by the decellularization processes.

MATERIALS AND METHODS

Valve preparation

Fresh porcine AVs were harvested from hearts obtained from a local slaughter house, placed into chilled phosphate buffered saline (PBS), and transported to the laboratory, then frozen temporarily in PBS at −80°C for later use. At time of testing, the AVs were quickly thawed, and the leaflets were dissected from the aortic root. The AVLs were then placed in a decellularization solution.

Decellularization methods

The following decellularization protocols, which were chosen due to their wide use, were utlized [19–22]:

1. *SDS*. Twelve AVLs were incubated in a hypotonic Tris buffer (10mmM Tris, PH 8.0) with 0.1% EDTA and 10 KIU/ml aprotinin for 1 hour and then decellularized with 0.1% SDS in same hypotonic Tris buffer, protease inhibitors, and RNase A (20μg/ml) and DNase (0.2 mg/ml). The decellularization lasted 48 hours at room temperature with constant shaking. The decellularized tissues were then washed in PBS [19,20].
2. *Trypsin*. Twelve AVLs were incubated under continuous shaking in Trypsin/EDTA (0.5% Trypsin and 0.2% EDTA) in hypotonic Tris buffer, together with RNase A (20μg/ml) and DNase (0.2 mg/ml) at 37°C for 48 hours. The Trypsin/EDTA solution was changed twice. Then the decellularized leaflets were washed under shaking conditions for removal of residual substances with PBS [22].
3. *Triton X-100*. Twelve AVLs were placed in a solution of 1% Triton X-100 with 0.2% EDTA (Sigma) in hypotonic Tris buffer for 48 hours, together with RNase A (20μg/ml) and DNase (0.2 mg/ml). All steps were conducted in a 5% CO_2/95% air atmosphere at 37°C under continuous shaking. The valves were washed with PBS several times to remove residual substances [21].

Planar biaxial testing

A detailed description of the biaxial testing device has been previously presented [29,30]. Briefly, a 10 mm × 10 mm square was dissected from the central belly region of the decellularized leaflet. Four fiducial markers were placed in the center of the square. Two loops of 000 nylon suture of equal length were attached to each side of the specimens with four stainless steel hooks. The specimens were then mounted onto the biaxial deice with the radial and circumferential directions aligned with the x_1 and the x_2 stretch axes of the device, respectively. All testing was performed with the specimen completely immersed in PBS (pH 7.4) at room temperature.

During testing, membrane tension (force/unit length) was applied along each axis and was ramped slowly from a pre-stress, ~0.5 N/m, to a peak value that depended upon the protocol using a triangular waveform. Specimens were first preconditioned for 10 contiguous cycles, following seven loading protocols: T_{cc}:T_{RR} = 10:60, 30:60, 45:60, 60:60, 60:45, 60:30, and 60:10 N/m, where T_{CC} and T_{RR} are the applied tensions in the circumferential and radial directions, respectively [2]. A peak tension of 60 N/m was used because it corresponds to in vivo diastolic pressure [1]. Net extensibility was characterized by areal strain under 60 N/m tension

$$(\lambda_{RR} \cdot \lambda_{CC} - 1) \times 100\,\%, \quad (1)$$

where λ_{rr} and λ_{cc} were the maximum stretches along radial and circumferential directions, respectively.

In addition to determining tissue extensibility, we also examined the maximum tangent moduli (MTM) at the peak tension of 60 N/m along the circumferential and radial axes. Due to the highly coupled behavior of aortic valve tissues [2,31], the MTM does not have a unique value but instead is highly dependent on the tissue loading state. We thus decided to determine MTM values for each axis using the specific test protocols wherein the loading along the axis was the greatest (i.e. T_{cc}:T_{rr} = 60:10 and T_{cc}:T_{rr} = 10:60 for the circumferential and radial directions, respectively). We also compared the inter-fiber mechanical interactions and fiber rotations, providing further insight into the structural changes caused by decellularization. As in our previous study [32] the degree of axial cross-coupling was defined as the percent change in peak stretch ratio along each axis, as the biaxial load was changed from equibiaxial (T_{CC}:T_{RR} = 1:1) to non-equibiaxial conditions (e.g. T_{CC}:T_{RR} = 1:0.17) and calculated by

$$\left(\frac{\Delta\lambda}{\lambda_{\mathrm{eq}}^{\mathrm{peak}}}\right)\times 100\ \%\ , \tag{2}$$

where λ_{peak}^{eq} was the peak stretch at 60 N/m and Δλ was the difference between the peak stretch at non-equibiaxial condition and λ_{peak}^{eq}

Flexural mechanical stiffness

Bending is also a major leaflet deformation mode in native [33] and bioprosthetic heart valves [34]. Moreover, exposing AVL to bidirectional flexural deformations will subject the AVL layers to tensile and compressive forces [33], allowing one to investigate the mechanical properties of the different layers of the AVL and how these properties were affected by decellularization. A detailed description of the bending device was previously presented [35, 36]. Briefly, rectangular strips were dissected from the central belly region, with the strips cut parallel to the circumferentially oriented collagen fibers. Each sample was marked with 3 fiducial graphite markers placed on the transmural surface of the sample with cyanoacrylate. The ventricularis was mounted upwards and the fibrosa faced the bottom of the bath. Hollow posts were mounted on both cross-sectional surfaces of a rectangular sample. Two anchor points, one placed on the fixed post and one placed on the bending bar were used as the final two markers used to compute the curvature. During testing, the fixed post was moved towards the bending bar. As the sample deformed, the bending bar deflected, which represented the amount of force exerted on the sample. The deformation was measured in terms of change of curvature calculated from the fiducial markers and two anchor points. Each specimen was flexed in two directions, with curvature (WC), which subjected the ventricularis to tension and against curvature (AC), which subjected the fibrosa to tension.

The overall effective stiffness was found by relating the moment and change of curvature to the flexural rigidity using the Euler-Bernoulli relationship:

$$M = E_{eff} I \Delta K. \tag{3}$$

This approach has been previously presented by Mirnajafi et al. [37]. Following this approach, the following exponential function was used

$$M(\Delta K) = a(1 - e^{-b\Delta K}). \tag{4}$$

Thus, the effective stiffness, E_{eff}, was computed using

$$E_{eff} = \frac{ab \cdot e^{-b\Delta k}}{I}, \quad (5)$$

where a and b are parameters determined by least squares fitting to the moment –curvature data.

Small angle light scattering (SALS) measurements

A detailed description of the SALS technique has been previously presented [38]. Briefly, a 4 mW HeNe continuous unpolarized laser (λ = 632.8 nm) was passed through the tissue specimen. The spatial intensity distribution of the resulting scattered light represented the sum of all structural information within the light beam envelope. The angular distribution of scattered light pattern, I(Φ), which represents distribution of fiber angles within light beam envelope, was obtained. Quantifiable information based on I(Φ) includes orientation index (OI) and preferred fiber direction (Φ_C). The orientation index (OI) was defined as the angle that contains one half of the total area under the I(Φ) distribution. Normalized orientation index (NOI) was calculated using:

$$NOI = \frac{90^\circ - OI}{90^\circ} \times 100\%, \quad (6)$$

where NOI ranged from 0% for a complete random network to 100% for a perfectly aligned network [38].

To prepare specimens for SALS testing, the leaflets were first fixed with glutaraldehyde in order to prevent tissue degradation during tissue preparation and fixation is required for histological preparation. The glutaraldehyde-fixed leaflets were dehydrated in graded solutions of glycerol/saline of 50, 75, 87, and 100% for an hour each. This process cleared the leaflets, which was necessary for accurate SALS measurements. It has been shown that the graded glycerol solution did not measurably distort the leaflet shape [39]. SALS measurements were then conducted over the entire leaflet surface in order to quantify the gross fiber structure of the leaflets. To quantify regional variations, the SALS data were subdivided into upper (Regions A and B) and lower (Regions C and D) commissure regions and upper (Regions 1, 2, and 3) and lower (Region 4 and 5) belly regions [39].

Histological and morphological analyses

The following histological analyses were performed to assess overall dimensional changes due to decellurization, verify that no cell nuclei was present, assess the degree of preservation of the leaflet trilayered structure, and to observe changes in the collagen crimp structure. Before and after decellularization of the AVLs, thickness measurements were taken with a dial caliper with an accuracy of ±0.0254 mm. Three thickness measurements were taken in the belly region, and two thickness measurements were taken in the commissure regions. The area of the valve leaflet was measured by plotting the leaflet contour and then quantifying with imaging software (Image Pro Plus) with an accuracy of ±0.1mm^2.

For histological analysis, transverse sections were cut from the belly regions, where the sections were aligned so that the long edge was parallel to the local preferred fiber direction. A hematoxylin and eosin (H&E) stain was used to validate that no cell nuclei was present after decellularization of the AVLs. To elucidate the trilayered leaflet structure, a Movat Pentachrome stain was used to identify collagen, elastin, and glycosaminoglycans with yellow, black and blue color, respectively. A picrosirius red stain was used to investigate the effects of decellularization on the collagen crimp structure. Under polarized light microscopy, collagen fibers of the AV displayed periodic light-distinguishing bands that corresponded to collagen crimp periods. All stained leaflet sections were imaged using bright field microscopy.

For scanning electron microscopy (SEM), a square section was dissected from the central belly region of the 3 different decellularized leaflets. The square section was then cut into 2 smaller squares, in order to examine the fibrosa of the first square and the ventricularis of the second square. Each section was fixed with 2.5% glutaraldehyde for 24 hours followed by three 15-minute washes in PBS. Then, each section was washed in sequential washes of 30%, 50%, 70%, 90%, and 100% ethanol. The specimens were left in each wash for 15 minutes and the 100% washed was performed 3 times. Next, specimens were subjected to critical point drying and gold sputter coating. Finally, SEM was used to view the ultrastructure of the fibrosa and the ventricularis of the decellularized leaflets.

Statistics

A Statistical analysis was performed with One Way Analysis of Variances (ANOVA) (SigmaStat 3.0, SPSS Inc., Chicago, IL). The Holm-Sidak Test, which can be used for pair wise comparisons and comparisons versus a control group, was used for the post hoc comparison. Results were considered significantly different at $p < 0.05$.

RESULTS

Mechanical properties

The net extensibility, represented by areal strain under 60 N/m equibiaxial tension, was found to increase after all three decellularization treatments when compared to the native AV [40] (Fig. 1-a). Among the three decellurization protocols, Triton X-100 showed the largest increase ($p=0.003$, Fig. 1-a). Maximum stretch ratios were evaluated in both the circumferential and the radial directions at 60 N/m equibiaxial tension (Fig. 1-b), which showed that Triton X-100 had the greatest effect on the extensibility in the radial direction ($p < 0.001$). Overall, the MTM of the radial direction was not affected by the decellularization process ($p = 0.736$, Fig. 2). However, the MTM of the circumferential direction was increased in tissue decellularized with Triton X-100 ($p=0.003$, Fig. 2). Mechanical coupling of the stretch axes was affected in all decellularization protocols (Fig. 3), indicative of tissue structural alterations. In general, all decellurization protocols induced larger changes in stretch along the opposite stretch axis. This is likely due to increased fiber mobility after decellularization resulting from a collagen network less bounded after decellularization.

All decellularization treatments were found to significantly affect the flexural behavior of valve leaflets. As in our previous study, native AVLs demonstrated a near linear moment-curvature relationship (Fig 4-a, [35]). However, the decellurized tissues did demonstrate a profound stiffness loss, which decreased with increasing flexure (Fig. 4-b). Moreover, this nonlinear response was observed when the specimen was flexed in both WC and AC directions (Fig. 4). The resulting moment-curvature response was fit well by equation (4) to determine E_{eff} ($\Delta\kappa$) (Table 1). To determine a mean specimen stiffness, E_{eff} at $\Delta\kappa=0.01$ was computed for each specimen based on the fit. The resulting E_{eff} of decellularized AVL was then compared with the native AV. The mean E_{eff} of the native AV was 156.0±24.6 kPa when flexed WC and 133.7 ±20.7 kPa when flexed AC.

Gross- and micro-structural characteristics

The gross collagen fiber structure was still preserved after decellularization (Fig. 5). Evaluation of tissue dimensions revealed that decellularization of the AV caused variable results. Decellularization with SDS did not cause any statistical differences ($p=0.192$) in area or thickness (Table 2). Decellularization with Trypsin caused tissue area and thickness dimensions to increase ($p=0.011$ and $p=0.002$, respectively (Table 2), and decellularization with Triton-X caused tissue area and thickness dimensions to decrease ($p \leq 0.001$ and $p \leq 0.001$, respectively) (Table 2).

SALS results for native AV exhibited significant regional variations of various degrees of alignment (Fig. 6). The region of coaptation and the mid belly region was aligned relatively well, whereas the region of the leaflet, which contained the Nodulus of Aranti, displayed poorer alignment (Fig. 6-a). The regional variations were preserved in the leaflets decellularized with SDS and Trypsin (Figs. 6-b,c), but were not preserved in leaflets decellularized with Triton X-100. The leaflets decellularized with Triton X-100 displayed a more homogenous fiber ultrastructure (Fig. 6-d). A regional analysis gave further insight into the regional variations of the decellularized leaflets. The analysis revealed that there were not significant differences between the native AV and the decellularized AVs, but, overall, decellularization caused a decrease in NOI values in each commissure and belly region (Table 3).

Histological results indicated no cell nuclei present after all three decellularization protocols (Figs. 6 b-d) as compared to the native AV (Fig. 7-a). The trilayered structure of the leaflet decellularized with SDS was very similar to the trilayered structure of the native AV (Figs. 7 e,f). However, the spongiosa was depleted with decellularization with Triton X-100 and Trypsin (Figs. 7-g, h). The macroscopically well-organized collagen crimp structure of the fibrosa was disrupted by all three decellularization protocols as compared to the native AV (Figs. 7 I–l). The collagen fibers were locally crimped (Fig. 7 j–l) but no longer showed macroscopic distinguishing bands (Fig. 7-i).

SEM

Comparing the fibrosa of all decellularized leaflets, SEM verified that leaflets decellularized with SDS preserved a dense collagen network (Fig. 8-b). Trypsin and Triton X-100's collagen networks were loose with large pores (Figs. 8-c, d). When comparing the ventricularis of all the decellularized leaflets, the same results were found (Figs. 8f–h). Overall, leaflets decellularized with SDS contained a dense ECM network similar to the ECM of the native AV (Figs. 8a, e), whereas, leaflets decellularized with Trypsin and Triton X-100, displayed a looser ECM network.

DISCUSSION

While heart valve tissue engineering has generated much interest, many unanswered questions remain and technical barriers must be overcome before widespread clinical application can be envisioned [41–43]. Normal heart valves are vital and dynamic tissues composed of specialized cells and ECM that respond and remodel in response to changes in local mechanical forces [42]. A successful TEHV and its components must accommodate repetitive changes in shape, dimension, and stress of the leaflet due to opening and closing of the valve leaflets. It must also have ongoing strength, flexibility, and durability, beginning at the instant of implantation and continuing indefinitely thereafter [41]. Thus, the goal of the current study was to provide insight into these long-term goals for the decellurization approach to TEHV. Understanding the mechanical and the microstructural effects caused by decellularization of the AV tissues and establishing functional limits are essential to the future development of a functional TEHV.

All decellularization protocols (SDS, Trypsin, and Triton X-100) induced an increase in leaflet extensibility, with Triton X-100 having the greatest affect on the radial extensibility (Figs. 1-a, b). This hypothesis is supported by the results for axial cross-coupling (Fig. 3a, b) which indicated larger radial strains for all protocols for decellurized tissues. It is known that the large radial strains in the native aortic valve are enabled by large rotations of the circumferentially oriented fibers rather than more extensible fibers aligned to the radial direction [2, 31]. Thus, increased radial extensibility was likely due to the increased ability for the circumferentially oriented collagen fibers to rotate in the decellurized tissue matrix. Along similar lines, the flexural behavior changed markedly after each decellularization protocol (Fig. 4). The nonlinear response and decrease in flexural rigidity was likely associated with ECM disruption.

Overall, all mechanical measurements were affected by decellularization. This implied that the decellularization process induced mechanical and microstructural defects.

Overall, decellurization did not change the gross appearance (Fig. 5) or collagen fiber network (Fig. 6) when compare do the native valve. This may give the initial impression that decellurization does little damage to the AV ECM. Yet, decellularization with Trypsin caused the tissue area and thickness dimentions increase and decellularization with Triton X-100 caused the tissue area and thickness dimensions to decrease (Table 2). Tissue stained with H&E demonstrated that there were no cells nuclei present after decellularization with all three protocols (Figs. 7 b–d), and a preserved the trilayered structure with SDS (Fig. 7-f). However, decellularization with Trypsin and Triton X-100 resulted in a depletion of the spongiosa layer (Fig. 7 g, h). It has been suggested that the principle function of the spongiosa is to dampen the vibrations in the fibrosa associated with leaflet flexion during closure [44]. Due to the loss of major GAG content in the spongiosa with decellularization of Trypsin and Triton X-100, early tissue degradation may result. Moreover, decellularization with Trypsin appeared to have induced a disruption of the elastin layer (Fig. 7-g), causing a loss of its organization.

Using picrosirius staining, decellurized AV tissue revealed a disruption of the collagen crimp structure when decellularized with each protocol (Fig. 7j–l) compared to the native AV (Fig. 7-i). The collagen fibers were locally crimped (Fig. 7j–l) but no longer showed the macroscopically organized light distinguishing bands (Fig. 7-i). This may have major implications on the long term tissue durability. Loss of collagen crimp indicates a loss of a protection mechanism, which prevents the collagen from being damaged during loading.

SEM revealed that tissues decellularized with SDS had a dense collagen network with a small pore size as opposed to the loose collagen network and increased pore size of tissues decellularized with Trypsin and Triton X-100 (Fig. 8b–d). Evaluation of the ventricularis revealed the same results (Figs. 8f–h). It has been hypothesized that normal tissue homeostasis was a function of aortic valve interstitial cells (AVIC) [45]. Although the ECM of SDS treated leaflets bore close resemblance to that of the native AV (Figs. 8a,e), the dense collagen network and small pore size may limit AVIC repopulation. If AVIC repopulation did not occur, the ECM will probably degrade over time, rendering the tissue scaffold nonfunctional.

In our experiments, heart valves were temporarily stored at −80 °C for testing. It has been demonstrated that short term storage at low temperature has minimal effects on mechanical properties of connective tissues.[46–48] A study also showed that freeze storage in saline solution only significantly changes the mechanical properties of collagenous tissue (tendon) for duration longer than 40 days.[49] Recently, Schenke-Layland et al. showed that certain local ultrastructural disruption was caused by one week cryopreservation using multiphoton laser scanning microscope.[50] Note that the structural deterioration after decellularization procedures were more aggressive than what observed in Schenke-Layland's study, in which conventional histology revealed almost comparable cell and ECM formations in fresh and cryopreserved valve leaflets.[50] Apparently, structural deterioration in our observation was caused by decellularization procedures instead of temporary freeze storage.

CONCLUSIONS

The potential for decellularized aortic heart valves (AVs) as heart valve replacements is based on the assumption that the major cellular immunogenic components have been removed, and that the remaining extracellular matrix (ECM) retains the necessary mechanical properties and functional design. In the present study we explored the effects of an anionic detergent (SDS), enzymatic agent (Trypsin), and a non-ionic detergent (Triton X-100) on the mechanical and structural properties of AV leaflets (AVLs) to provide greater insight into the initial functional

state of the decellularized AVL. Overall, SDS appeared to maintain critical mechanical and microstructural properties. However, SEM suggested that although the ECM of SDS treated leaflets resembled that of the native AV, AVIC repopulation may not be optimal due to a dense ECM network and a small pore size. While the overall fiber architecture remained relatively unchanged, polarized light imaging and SEM revealed that decellularization resulted in substantial disruption of collagen network. In conclusion, changes in mechanical and structural properties of decellularized leaflets were likely associated with disruption of the ECM, which may impact the durability of the leaflets.

Acknowledgements

This work is supported by a Beginning Grant-in-Aid (0565346U) from the American Heart Associate (Pennsylvania/Delaware Affiliate) to JL. The authors would like to thank Jennifer Debarr of the McGowan Institute and Mark Rubin of Center for Biologic Imaging for their assistance with histology and SEM.

References

1. Thubrikar, M. The Aortic Valve. Boca Raton: CRC; 1990. p. 221
2. Billiar KL, Sacks MS. Biaxial mechanical properties of the natural and glutaraldehyde treated aortic valve cusp--Part I: Experimental results. Journal of Biomechanical Engineering 2000a;122(1):23–30. [PubMed: 10790826]
3. Schoen F, Levy R. Tissue heart valves: Current challenges and future research perspectives. Journal of Biomedical Materials Research 1999;47:439–465. [PubMed: 10497280]
4. Senthilnathan V, Treasure T, Grunkemeier G, Starr A. Heart valves: which is the best choice? Cardiovasc Surg 1999;7(4):393–7. [PubMed: 10430519]
5. Sacks MS, Enomoto Y, Graybill JR, Merryman WD, Zeeshan A, Yoganathan AP, Levy RJ, Gorman RC, Gorman JH 3rd. In-vivo dynamic deformation of the mitral valve anterior leaflet. Ann Thorac Surg 2006;82(4):1369–77. [PubMed: 16996935]
6. Hoerstrup SP, Sodian R, Daebritz S, Wang J, Bacha EA, Martin DP, Moran AM, Guleserian KJ, Sperling JS, Kaushal S, Vacanti JP, Schoen FJ, Mayer JE Jr. Functional living trileaflet heart valves grown In vitro. Circulation 2000;102(19 Suppl 3):III44–9. [PubMed: 11082361]
7. Stock UA, Vacanti JP, Mayer JE Jr, Wahlers T. Tissue engineering of heart valves -- current aspects. Thorac Cardiovasc Surg 2002;50(3):184–93. [PubMed: 12077696]
8. Dahm M, Lyman WD, Schwell AB, Factor SM, Frater RW. Immunogenicity of glutaraldehyde-tanned bovine pericardium. J Thorac Cardiovasc Surg 1990;99(6):1082–90. [PubMed: 2141662]
9. Valente M, Bortolotti U, Thiene G. Ultrastructural substrates of dystrophic calcification in porcine bioprosthetic valve failure. Am J Pathol 1985;119(1):12–21. [PubMed: 3985118]
10. Levy RJ, Schoen FJ, Flowers WB, Staelin ST. Initiation of mineralization in bioprosthetic heart valves: studies of alkaline phosphatase activity and its inhibition by AlCl3 or FeCl3 preincubations. J Biomed Mater Res 1991;25(8):905–35. [PubMed: 1918108]
11. Rossi MA, Braile DM, Teixeira MD, Souza DR, Peres LC. Lipid extraction attenuates the calcific degeneration of bovine pericardium used in cardiac valve bioprostheses. J Exp Pathol (Oxford) 1990;71(2):187–96. [PubMed: 2331406]
12. Schoen F, Levy R, Nelson A, Bernhard W, Nashef A, Hawley M. Onset and progression of experimental bioprosthetic heart valve calcification. Laboratory Investigations 1985;52(5):523–532.
13. Courtman DW, Pereira CA, Kashef V, McComb D, Lee JM, Wilson GJ. Development of a pericardial acellular matrix biomaterial: Biochemical and mechanical effects of cell extraction. Journal of Biomedical Materials Research 1994;28:655–666. [PubMed: 8071376]
14. Jorge-Herrero E, Getierrez MP, Castillo-Olivares JL. Calcification of soft tissue employed in the construction of heart valve prostheses:Study of different chemical treatements. Biomaterials 1991;12:249–252. [PubMed: 1878460]
15. Steinhoff G, Stock U, Karim N, Mertsching H, Timke A, Meliss RR, Pethig K, Haverich A, Bader A. Tissue engineering of pulmonary heart valves on allogenic acellular matrix conduits: in vivo restoration of valve tissue. Circulation 2000;102(19 Suppl 3):III50–5. [PubMed: 11082362]

16. Wilson GJ, Courtman DW, Klement P, Lee JM, Yeger H. Acellular matrix: a biomaterials approach for coronary artery bypass and heart valve replacement. Ann Thorac Surg 1995;60(2 Suppl):S353–8. [PubMed: 7646187]

17. Courtman DW, Pereira CA, Omar S, Langdon SE, Lee JM, Wilson GJ. Biomechanical and ultrastructural comparison of cryopreservation and a novel cellular extraction of porcine aortic valve leaflets. J Biomed Mater Res 1995;29(12):1507–16. [PubMed: 8600141]

18. Zeltinger J, Landeen LK, Alexander HG, Kidd ID, Sibanda B. Development and characterization of tissue-engineered aortic valves. Tissue Eng 2001;7(1):9–22. [PubMed: 11224920]

19. Booth C, Korossis SA, Wilcox HE, Watterson KG, Kearney JN, Fisher J, Ingham E. Tissue engineering of cardiac valve prostheses I: development and histological characterization of an acellular porcine scaffold. J Heart Valve Dis 2002;11(4):457–62. [PubMed: 12150290]

20. Korossis SA, Booth C, Wilcox HE, Watterson KG, Kearney JN, Fisher J, Ingham E. Tissue engineering of cardiac valve prostheses II: biomechanical characterization of decellularized porcine aortic heart valves. J Heart Valve Dis 2002;11(4):463–71. [PubMed: 12150291]

21. Bader A, Schilling T, Teebken OE, Brandes G, Herden T, Steinhoff G, Haverich A. Tissue engineering of heart valves--human endothelial cell seeding of detergent acellularized porcine valves. Eur J Cardiothorac Surg 1998;14(3):279–84. [PubMed: 9761438]

22. Cebotari S, Mertsching H, Kallenbach K, Kostin S, Repin O, Batrinac A, Kleczka C, Ciubotaru A, Haverich A. Construction of autologous human heart valves based on an acellular allograft matrix. Circulation 2002;106(12 Suppl 1):I63–I68. [PubMed: 12354711]

23. Shinoka T, Breuer CK, Tanel RE, Zund G, Miura T, Ma PX, Langer R, Vacanti JP, Mayer JE Jr. Tissue engineering heart valves: valve leaflet replacement study in a lamb model. Ann Thorac Surg 1995;60(6 Suppl):S513–6. [PubMed: 8604922]

24. Sodian R, Hoerstrup SP, Sperling JS, Daebritz S, Martin DP, Moran AM, Kim BS, Schoen FJ, Vacanti JP, Mayer JE Jr. Early In vivo experience with tissue-engineered trileaflet heart valves. Circulation 2000;102(19 Suppl 3):III22–9. [PubMed: 11082357]

25. Bertipaglia B, Ortolani F, Petrelli L, Gerosa G, Spina M, Pauletto P, Casarotto D, Marchini M, Sartore S. Cell characterization of porcine aortic valve and decellularized leaflets repopulated with aortic valve interstitial cells: the VESALIO Project (Vitalitate Exornatum Succedaneum Aorticum Labore Ingenioso Obtenibitur). Ann Thorac Surg 2003;75(4):1274–82. [PubMed: 12683575]

26. Grabow N, Schmohl K, Khosravi A, Philipp M, Scharfschwerdt M, Graf B, Stamm C, Haubold A, Schmitz KP, Steinhoff G. Mechanical and structural properties of a novel hybrid heart valve scaffold for tissue engineering. Artif Organs 2004;28(11):971–9. [PubMed: 15504112]

27. Stamm C, Khosravi A, Grabow N, Schmohl K, Treckmann N, Drechsel A, Nan M, Schmitz KP, Haubold A, Steinhoff G. Biomatrix/polymer composite material for heart valve tissue engineering. Ann Thorac Surg 2004;78(6):2084–93. [PubMed: 15561041]

28. Spina M, Ortolani F, Messlemani AE, Gandaglia A, Bujan J, Garcia-Honduvilla N, Vesely I, Gerosa G, Casarotto D, Petrelli L, Marchini M. Isolation of intact aortic valve scaffolds for heart-valve bioprostheses: extracellular matrix structure, prevention from calcification, and cell repopulation features. J Biomed Mater Res A 2003;67(4):1338–50. [PubMed: 14624521]

29. Sacks MS, Chuong CJ. Orthotropic mechanical properties of chemically treated bovine pericardium. Ann Biomed Eng 1998;26(5):892–902. [PubMed: 9779962]

30. Sacks MS. A method for planar biaxial testing that includes in-plane shear. Journal of Biomechanical Engineering 1999;121:551–555. [PubMed: 10529924]

31. Billiar KL, Sacks MS. Biaxial mechanical properties of the native and glutaraldehyde-treated aortic valve cusp: Part II--A structural constitutive model. Journal of Biomechanical Engineering 2000b; 122(4):327–35. [PubMed: 11036555]

32. Wells SM, Sacks MS. Effects of fixation pressure on the biaxial mechanical behavior of porcine bioprosthetic heart valves with long-term cyclic loading. Biomaterials 2002;23(11):2389–99. [PubMed: 12013187]

33. Huang HYS, Liao J, Sacks MS. Effects of transvalvular pressure on aortic valve interstitial cell nuclear aspect ratio. Journal of Biomechanial Engineering. in-press

34. Iyengar AKS, Sugimoto H, Smith DB, Sacks MS. Dynamic in vitro quantification of bioprosthetic heart valve leaflet motion using structured light projection. Ann Biomed Eng 2001;29(11):963–73. [PubMed: 11791679]
35. Lam, TV.; Sacks, MS. Transmural strains of heart valve tissues under flexure. Annual Biomedical Engineering Society Fall meeting; Nashville, TN. 2003.
36. Lovekamp JJ, Simionescu DT, Mercuri JJ, Zubiate B, Sacks MS, Vyavahare NR. Stability and function of glycosaminoglycans in porcine bioprosthetic heart valves. Biomaterials 2006;27(8): 1507–18. [PubMed: 16144707]
37. Mirnajafi A, Raymer J, Scott MJ, Sacks MS. The effects of collagen fiber orientation on the flexural properties of pericardial heterograft biomaterials. Biomaterials 2005;26(7):795–804. [PubMed: 15350785]
38. Sacks MS, Smith DB, Hiester ED. A small angle light scattering device for planar connective tissue microstructural analysis. Ann Biomed Eng 1997;25(4):678–89. [PubMed: 9236980]
39. Sacks MS, Smith DB, Hiester ED. The aortic valve microstructure: effects of transvalvular pressure. Journal of Biomedical Materials Research 1998;41(1):131–41. [PubMed: 9641633]
40. Stella JA, Sacks MS. On the biaxial mechanical properties of the layers of the aortic valve leaflet. J Biomech Eng 2007;129(5):757. [PubMed: 17887902]
41. Mendelson, KaSFJ. Heart Valve Tissue Engineering: Concepts, Approaches, Progress, and Challenges. Annals of Biomedical Engineering 2006;34(12):1799–1819. [PubMed: 17053986]
42. Schoen FJ. New frontiers in the pathology and therapy of heart valve disease: 2006 Society for Cardiovascular Pathology, Distinguished Achievement Award Lecture, United States-Canadian Academy of Pathology, Atlanta, GA, February 12, 2006. Cardiovasc Pathol 2006;15(5):271–9. [PubMed: 16979034]
43. Vesely I. Heart Valve Tissue Engineering. Circulation Research 2005;97:743–755. [PubMed: 16224074]
44. Konduri, S. Chemical Engineering. Georgia Institute of Technology; Atlanta: 2005. The Influence of Normal Physiological Forces on Porcine Aortic Heart Valves in a Sterile Ex Vivo Pulsatile Organ Culture System; p. 205
45. Taylor PM, Allen SP, Dreger SA, Yacoub MH. Human cardiac valve interstitial cells in collagen sponge: a biological three-dimensional matrix for tissue engineering. Journal of Heart Valve Disease 2002;11(3):298–306. [PubMed: 12056719]discussion 306–7
46. Woo SLY, Orlando CA, Camp JF, Akeson WH. Effects of Postmortem Storage by Freezing on Ligament Tensile Behavior. Journal of Biomechanics 1994;19:399–404. [PubMed: 3733765]
47. Moon DK, Woo SL, Takakura Y, Gabriel MT, Abramowitch SD. The effects of refreezing on the viscoelastic and tensile properties of ligaments. J Biomech 2006;39(6):1153–7. [PubMed: 16549103]
48. Pegg DE. The preservation of tissues for transplantation. Cell Tissue Bank 2006;7(4):349–58. [PubMed: 16957871]
49. Ng BH, Chou SM, Lim BH, Chong A. The changes in the tensile properties of tendons after freeze storage in saline solution. Proc Inst Mech Eng [H] 2005;219(6):387–92.
50. Schenke-Layland K, Madershahian N, Riemann I, Starcher B, Halbhuber KJ, Konig K, Stock UA. Impact of cryopreservation on extracellular matrix structures of heart valve leaflets. Ann Thorac Surg 2006;81(3):918–26. [PubMed: 16488695]

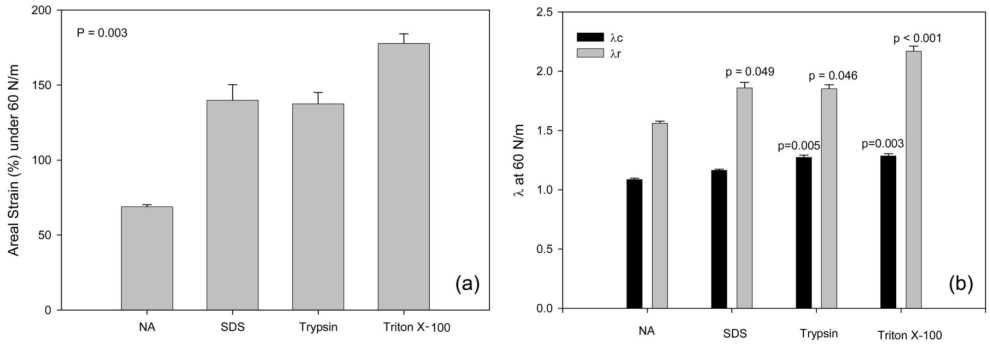

Figure 1.

Changes in AV tissue extensibility under 60 N/m equibiaxial tension for (a) areal strain and (b) peak stretch (λ) ratios in the circumferential and radial directions. Net extensibility increased for all decellularization protocols, with the leaflets treated with Triton X-100 exhibiting the greatest increase.

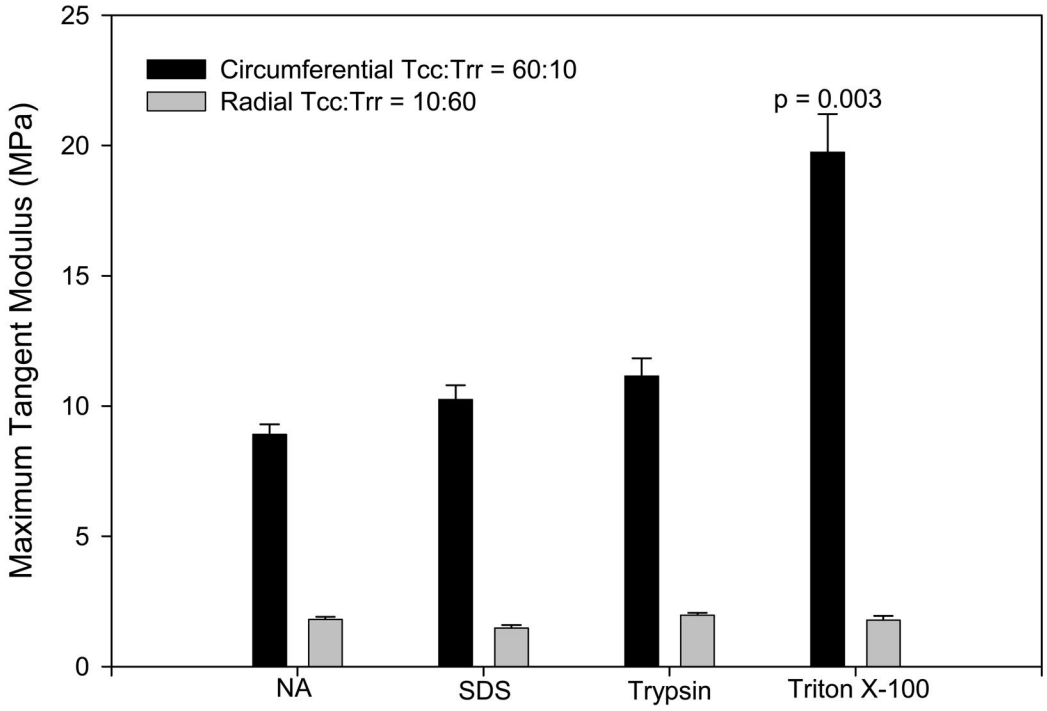

Figure 2.
Maximum tangent modulus (MTM) 60 N/m equibiaxial tension. Overall, each decellularization protocol increased the tangent modulus in the circumferential direction, with Triton X-100 causing the most significant increase. The tensile modulus of the radial direction was not affected by the decellularization process.

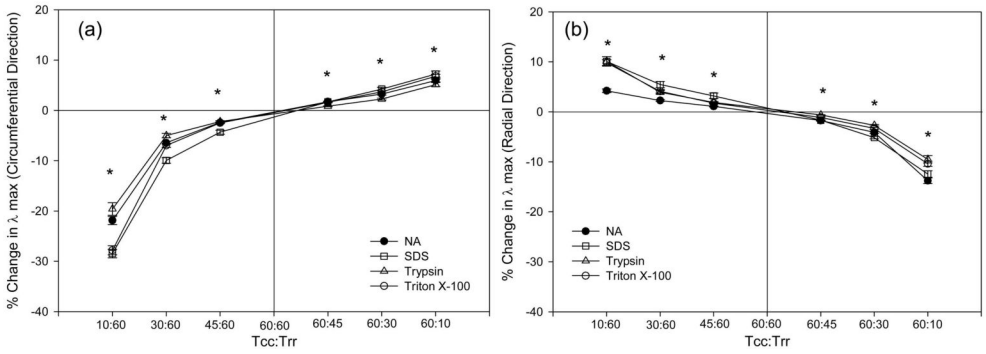

Figure 3.

Axial cross-coupling for the entire range of biaxial protocols for the (a) the circumferential and (b) the radial directions. All decellularization protocols induced significant changes indicative of subtle structural alterations in the tissue structure with the decellularization.

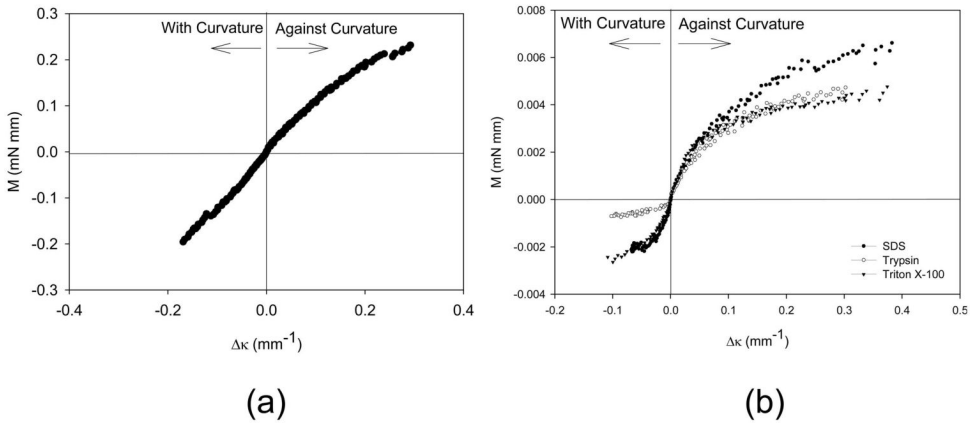

Figure 4.

Flexural behavior of for the (a) native valve and (b) decellurized leaflets (note carefully the different scales used for the moment axis). While the native tissue exhibited a linear response over the entire bending range, decellularized valve leaflets demonstrated a nonlinear response in both WC and AC directions. All decellularization protocols induced a large decrease in flexural rigidity, with the nonlinear response of flexural rigidity was likely associated with loss of stiffness and ECM disruption.

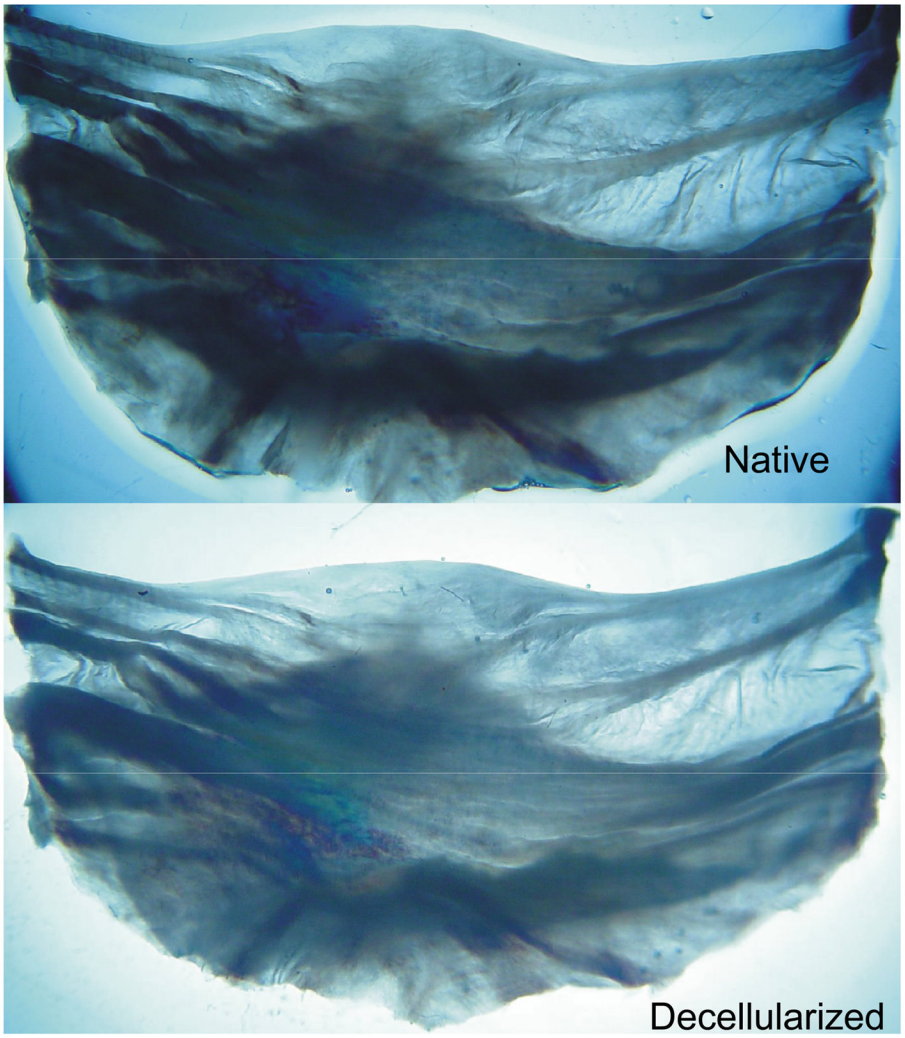

Figure 5.
Representative AV leaflets in the native and decellurized (using SDS, an anionic detergent) states, showing how the overall structure was preserved after decellularization.

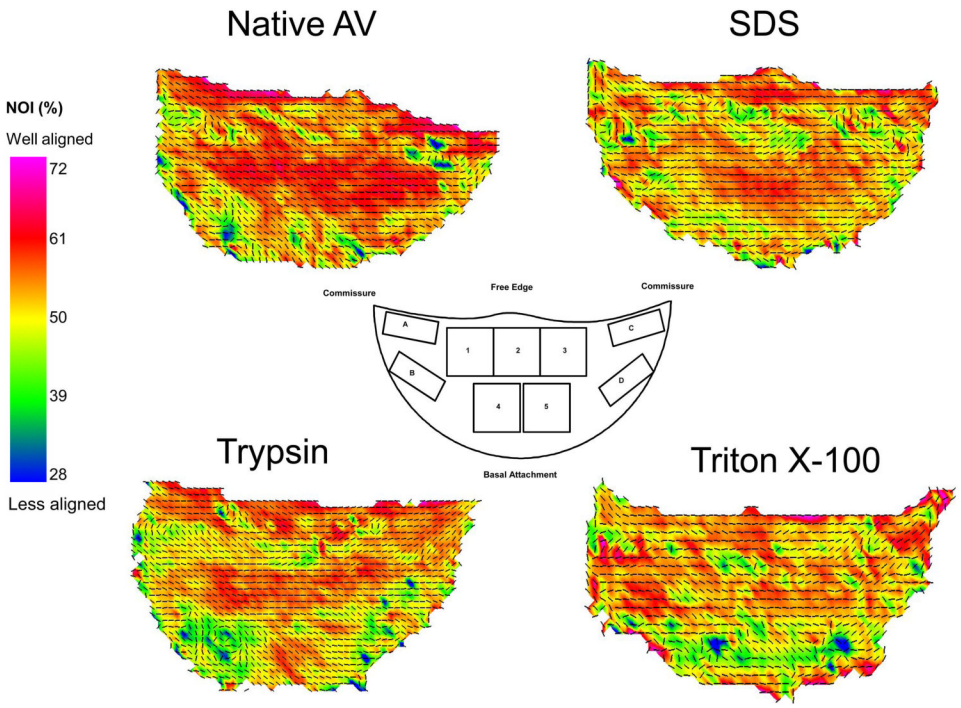

Figure 6.
Representative SALS results for the native AV and decellurized tissues. Overall, these quantitative changes demonstrated that the gross collagen fiber architecture was preserved after decellurization. Inset – definition of regions used for comparisons in decellurization protocols.

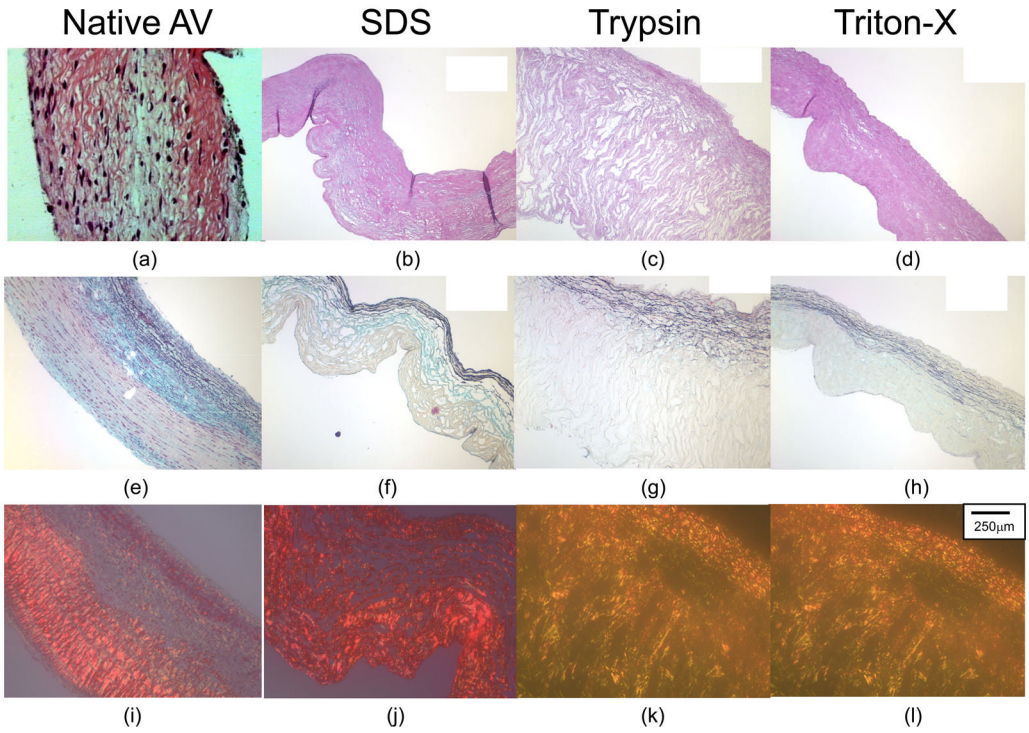

Figure 7.

Histology results using for (a–d) Hematoxylin and Eosin (H&E), (e–h) Movats Pentachrome, and (i–l) picrosirius stains. It is apparent that each decellularization protocol efficiently removed all cells. The trilayered structure of the leaflet decellularized with (f) SDS (anionic detergent) was very similar to the trilayered structure of the (e) native AV. However, the spongiosa was depleted with decellularization with (g) Trypsin (enzymatic agent) and (h) Triton X-100 (non-ionic detergent). Also, the collagen of the leaflets decellularized with Trypsin and Triton X-100 appeared to be degraded. The fibrosa layer in each of these tissues was not stained as intensely as the fibrosa layer of the tissue decellularized with SDS and the native AV, which may indicate collagen degradation. The elastin appeared to have lost some of its organization when compared to the native AV, possibly due to changes in tissue dimensions. (i–l) The macroscopically well-organized collagen crimp structure was disrupted by all three decellularization protocols as compared to the native AV. Again, collagen degradation had apparently occurred with Trypsin and Triton X-100 decellularization protocols.

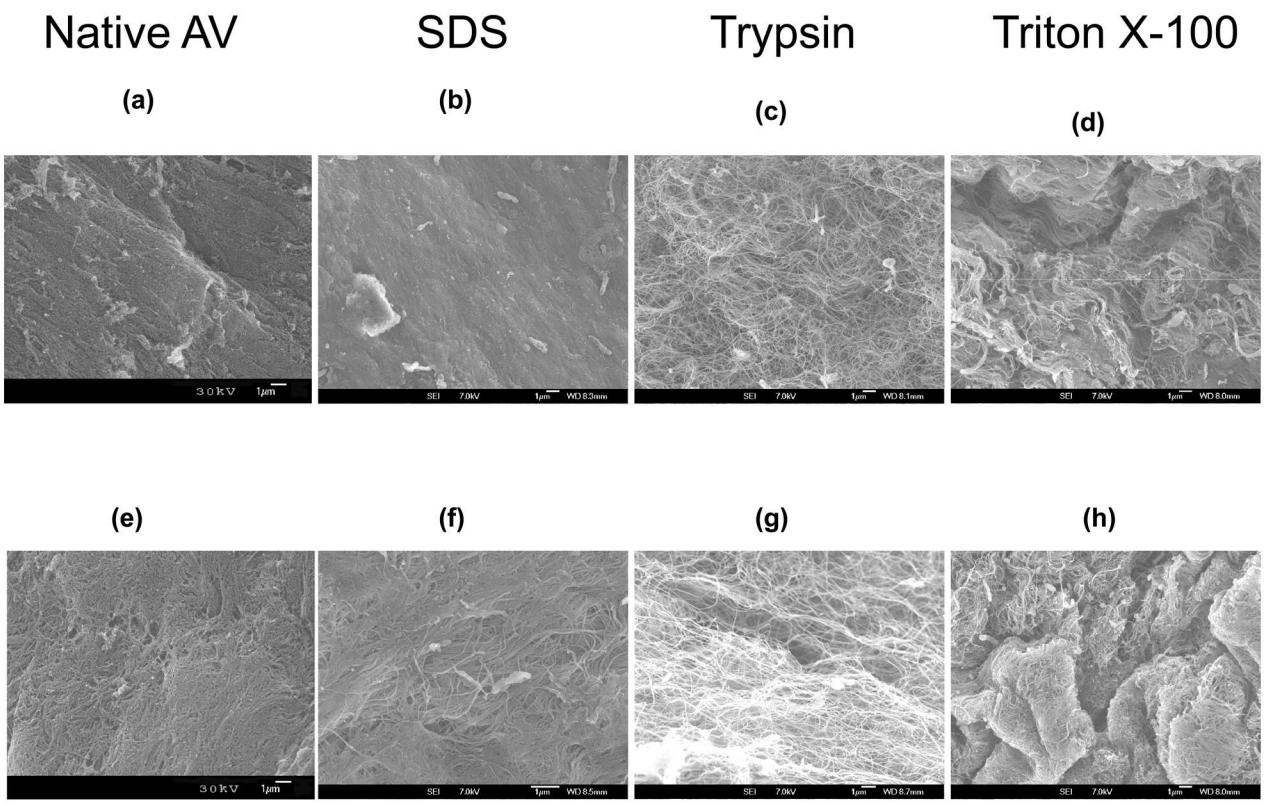

Figure 8.

SEM results for (a–c) the Fibrosa and (d–f) the ventricularis. Comparing the fibrosa of all decellularized leaflets, SEM verified that leaflets decellularized with (a), (d) SDS preserved a dense collagen network and small pore size. (b), (e) Trypsin and (c), (f) Triton X-100's collagen networks were loose with large pores. Due to the dense network and small pore size, AVIC repopulation may not occur well in SDS treated leaflets.

Table 1

Flexure stiffness results for native and decellurized AV leaflet tissues, demonstrating a large decrease of flexural stiffness for all decellularization protocols.

E_{eff} (kPa)	Native (n=18)	SDS (n=12)	Trypsin (n=11)	Triton X-100 (n=11)
WC (Ventricularis in Tension)	156.0 ± 24.6	23.5 ± 5.8	15.6 ± 4.8	19.4 ± 8.9
AC (Fibrosa in Tension)	133.7 ± 20.7	24.9 ± 12.8	47.4 ± 16.3	28.9 ± 6.5

Table 2

Changes in decellularization induced tissue dimensions. While overall area and thickness measurements after SDS treatment remained the same, decellularization with Trypsin caused tissue area and thickness dimensions to increase and decellularization with Triton-X caused tissue area and thickness dimensions to decrease. Values are given as mean±sem.

	Area of Valve Leaflets (mm^2)		Thickness of Valve Leaflets (mm)	
	Before Decellularization	After Decellularization	Before Decellularization	After Decellularization
SDS	264.5 ± 36.8	268.0 ± 35.9	0.48 ± 0.07	0.43 ± 0.08
Trypsin	250.5 ± 42.4	302.8 ± 49.6*	0.43 ± 0.04	0.48 ± 0.04*
Triton X- 100	260.9 ± 36.3	213.2 ± 26.6*	0.31 ± 0.05	0.16 ± 0.04*

Table 3

SALS NOI values for the commissure (A-D) and belly (1–5) regions (See Fig. 6, inset) of the decellularized AV leaflet tissues. NOI values are given as mean±sem. Overall, changes in gross collagen fiber architecture with decellurization were small.

Region	A	B	C	D	1	2	3	4	5
Native AV	53.84±1.71	51.47±0.19	56.54±1.91	52.02±3.30	56.74±1.42	52.72±3.22	53.45±3.49	55.37±2.65	54.41±6.18
SDS	51.39±1.34	49.52±1.49	54.90±0.39	51.31±2.06	53.90±1.73	51.03±2.79	52.12±0.65	55.86±1.44	56.77±0.41
Trypsin	53.49±1.92	50.42±2.77	54.16±2.59	49.22±5.19	51.42±2.55	47.58±3.97	53.48±2.39	52.60±1.27	52.46±0.37
Triton X-100	50.22±0.46	52.43±1.05	51.51±6.14	50.61±0.58	51.31±1.71	50.79±2.28	50.89±2.42	47.67±0.16	50.14±1.57